Open boundary conditions in stratified ocean models

Tommy G. Jensen [a,b,*]

[a] *Department of Atmospheric Science, Colorado State University, Fort Collins, CO 80523, USA*
[b] *International Research Centre for Computational Hydrodynamics, Danish Hydraulic Institute, Hørsholm, Denmark*

Abstract

In most applications of numerical ocean models, artificial boundaries are introduced to limit the domain. Along such a boundary we need to apply what is often referred to as an open boundary condition (OBC). In this paper a number of local methods used in barotropic ocean models are applied and discussed for the stratified case using a normal mode approach. The OBCs are the simple conditions: clamped, prescribed and zero gradient; the radiation conditions: Camerlengo–O'Brien, Orlanski and a method of characteristics based on linear equations; and a sponge type condition: the flow relaxation scheme. The OBCs have been implemented in a 3-layer ocean model and examples of how the various OBCs perform for three simple flow situations are investigated. The cases are: internal wave radiation, a quasi-steady coastal jet and the response to a storm moving across a strait. It is found that the flow relaxation scheme and the method based on characteristics perform well for the test cases in general, although some of the simpler methods give better results in individual cases. © 1998 Elsevier Science B.V. All rights reserved.

Keywords: oceanography; hydrodynamic; mathematical model; finite difference

1. Introduction

Numerical simulations of real oceanic flows will in most cases have an artificial boundary which consists of open water. The only exceptions are models of lakes, land-locked seas and the global ocean. Along such an artificial or non-physical boundary, inflow and outflow can occur and waves propagate into, or out, of the model domain. A wide range of time scales are of interest in the modelling of stratified seas, ranging from quasi-steady circulations to internal waves with periods of an hour or

less. This makes it difficult to treat all flows with the same method. However, if one can choose the position of the artificial boundary such that it simplifies the physics, a number of methods are available. This requires that the nature of the equations does not change, e.g. from being hyperbolic in nature to parabolic or elliptic in the vicinity of the artificial boundary. It should be emphasized that a perfect artificial boundary condition does not exist. In fact, it has be shown (e.g. Oliger and Sundström, 1978) that adding such conditions to the primitive equations may cause the combined problem to be ill-posed; thus a unique solution does not exist. This means that in general a ''best'' artificial boundary condition cannot be determined. Consequently, a more prag-

* Corresponding author. Fax: +1 970 491 8428; e-mail: jensen@neptune.atmos.colostate.edu

matic approach to artificial boundaries is used, where the actual method applied depends on the physics of the problem considered.

In the literature, different terminologies are used for artificial boundaries depending on the scientific discipline and on the nature of the flow problem. For instance, the term ''free'' boundary is often used when there is no forcing along such a boundary. For problems which include waves, the term ''non-reflecting'' boundary is often used (Givoli, 1991, 1992). If waves are only allowed to leave the domain, the term ''absorbing'' boundary has been used (Engquist and Majda, 1977). We will refer to a general artificial boundary as an ''open'' boundary, the term most frequently used for atmospheric and oceanic applications.

The topic of open boundary conditions (OBCs) has received much attention in numerical fluid dynamics, in particular for the Euler equations. For linear hyperbolic systems, Engquist and Majda (1977) proposed approximation methods of successively increasing order. Using third order schemes in time and space, they obtained solutions with very low reflection coefficients for surface gravity waves with normal as well as oblique incidence on the open boundary. However, their schemes are computationally expensive and must be reformulated depending on the flows, which makes them less attractive. A more general approach is to apply the method of characteristics to hyperbolic systems (e.g. Thompson, 1987, 1990). Poinsot and Lele (1992) extended this procedure to the Navier–Stokes equations and discussed in detail the complications involved in applying boundary conditions to the multi-dimensional case. They point out that non-reflecting boundary conditions for one-dimensional flows cannot easily be extended to two or three dimensions. One physical boundary condition they recommend, however, is to relax towards the pressure at infinity when appropriate. Boundary conditions for the remaining variables are computed from the interior using modified equations. A review of the general literature on OBCs in fluid mechanics is given by Givoli (1992).

The literature specific to oceanic and atmospheric problems is rather limited and the studies have been concentrated on the shallow water equations. A number of investigators (e.g. Camerlengo and O'Brien, 1980; Beardsley and Haidvogel, 1981; Røed and Smedstad, 1984; Chapman, 1985; Røed and Cooper, 1986, 1987; Martinsen and Engedahl, 1987) worked with linear, depth-integrated ocean models.

For the stratified ocean, the problem is fully three-dimensional and becomes more complicated. Near the surface, momentum advection is often very important, making the solution non-linear, and internal waves can propagate vertically as well as horizontally. In order to apply the techniques developed for barotropic models to the stratified case, we will only consider motion with a small aspect ratio, i.e. the horizontal scale of the motion is much larger than the vertical scale. In that case, one method is to project the solution on vertical normal modes (Jensen, 1993). In that work, a radiation condition was applied separately to each vertical mode and then transformed back to physical space. For models with a limited number of layers (or levels) this is computationally feasible and may be applied to any OBC.

Secondly, our philosophy in this paper is to primarily investigate the simplest and most commonly used OBCs. Consequently, we will concentrate on a small, but representative number of OBCs reviewed and tested by Chapman (1985) and Røed and Cooper (1987) for barotropic models. In their work the following OBCs were applied to the surface elevation: clamped (CLP) and zero gradient (GRD). For the velocity field, one-dimensional free wave radiation conditions were applied: Orlanski (OL) (i.e. Orlanski, 1976; Miller and Thorpe, 1981) and Camerlengo and O'Brien (1980), referred to as CO. A sponge condition (SPO) for velocity (Israeli and Orzag, 1981) and a method of characteristics (CHA) by Hedstrom (1979) were also investigated. In addition, a forced wave radiation condition, (Røed and Smedstad, 1984) and a two-dimensional free wave radiation condition (Raymond and Kuo, 1984) were included by Røed and Cooper (1987), but equivalent conditions for the stratified case will not be considered in this work. Given the many difficulties associated with OBCs for three-dimensional flows, we will also examine the flow relaxation scheme (FRS) as an open boundary condition. This was adopted for a barotropic ocean model by Martinsen and Engedahl (1987) and later applied to a stratified ocean (Cooper and Thompson, 1989; Slørdal et al., 1994; Engedahl, 1995).

A 3-layer model will be used to investigate three cases, inspired by the cases used by Chapman (1985) and Røed and Cooper (1987). The first is an internal wave radiation case where propagation is allowed only along one horizontal coordinate. With no rotation, this represents the simplest possible free internal wave propagation test. The second test is a coastal jet along a straight coast, forced by a wind stress uniform in the alongshore direction. This is a simple accelerating flow, representing a quasi-steady circulation. The last case is a more realistic problem, where a moving storm is crossing an infinitely long channel.

Radiation boundary conditions have in a few cases been applied to stratified ocean models. In the UK FRAM model, Stevens (1991) used an Orlanski-type phase velocity to modify advection of tracers. Oey and Chen (1992) applied a one-dimensional radiation condition to momentum, using a prescribed wave propagation speed close to the first baroclinic mode. In limited area modelling applications of the Bryan–Cox model, restoring zones towards climatology have been used for temperature and salinity (e.g. Sarmiento, 1986; Semtner and Chervin, 1992). For instance, in a recent high resolution (1/6 deg) study of the North Atlantic, the Newtonian damping time scale varied linearly from 5 to 50 days over 4/3 deg, (Beckmann et al., 1994). This technique corresponds to a sponge layer with relaxation to observations and is equivalent to the FRS (Martinsen and Engedahl, 1987).

2. The ocean model

The multi-layer ocean model by Jensen (1991, 1993), modified to include bottom topography (Jensen, 1996), is used here in a local Cartesian coordinate system. We assume that the x-axis points towards the east, the y-axis points towards the north and the vertical z-axis is upward. Depending on the problem to be considered, we will either ignore rotation or use the f-plane approximation, i.e. the Coriolis parameter is assumed constant.

Consider an ocean consisting of N layers of uniform density as shown in Fig. 1. The layers are labelled with increasing numbers downward. Let us assume that all layers have a positive thickness
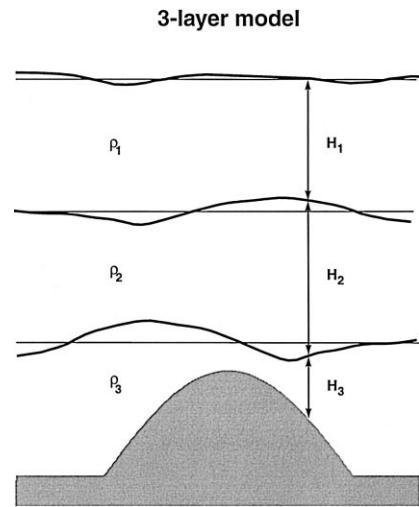

3-layer model

Fig. 1. Vertical structure of the 3-layer isopycnal model. Layer j has a constant density ρ_j and instantaneous thickness H_j. For the model runs in this paper each layer is on average 100 m thick. In the case of a storm over a channel, however, a shallow bank with a height of 80 m over the bottom is present as shown.

everywhere. This implies that layers are not allowed to surface or merge, and that the bottom topography is always in the lowest layer.

Let the velocity components toward the east and north be u and v, respectively. We choose $z = 0$ to be the surface of the ocean at rest. Define vertically integrated volume transport components U_j and V_j by:

$$U_j = \int_{z_j}^{z_{j+1}} u \, \mathrm{d}z \tag{1}$$

between two isopycnal surfaces $z_j(x,y,t)$ and $z_{j+1}(x,y,t)$, with an equivalent expression for V_j. The thickness of layer j defined by this integration, is $H_j = (z_{j+1} - z_j)$ and the vertically averaged density is ρ_j. The transport equation for U_j becomes:

$$\frac{\partial U_j}{\partial t} + \frac{\partial}{\partial x}\left(\frac{U_j^2}{H_j}\right) + \frac{\partial}{\partial y}\left(\frac{U_j V_j}{H_j}\right) - fV_j$$
$$= -gH_j \frac{\partial \Phi_j}{\partial x} + F_j^x + \frac{\tau_j^{x,t}}{\rho_j} - \frac{\tau_j^{x,b}}{\rho_j} \tag{2}$$

where the lateral friction term is given by:

$$F_j^x = H_j \left(A\nabla^2 - A_4 \nabla^4 \right)\left(\frac{U_j}{H_j}\right) \tag{3}$$

with a harmonic diffusivity A and biharmonic diffusivity A_4. Similarly for V_j, we have:

$$\frac{\partial V_j}{\partial t} + \frac{\partial}{\partial x}\left(\frac{U_j V_j}{H_j}\right) + \frac{\partial}{\partial y}\left(\frac{V_j^2}{H_j}\right) + fU_j$$

$$= -gH_j \frac{\partial \Phi_j}{\partial y} + F_j^y + \frac{\tau_j^{y,t}}{\rho_j} - \frac{\tau_j^{y,b}}{\rho_j} \qquad (4)$$

with:

$$F_j^y = H_j\left(A\nabla^2 - A_4\nabla^4\right)\left(\frac{V_j}{H_j}\right) \qquad (5)$$

In the equations above g is the acceleration of gravity, while τ is the tangential stress due to vertical friction. The superscripts on τ denote the x or y component and t or b refers to the top or bottom interface of the layer. The vertical stress for the x-direction at the top of each layer is:

$$\tau_j^{x,t} = \tau_w^x \delta_{1j} + \rho_j A_z\left(\frac{U_{j-1}}{H_{j-1}} - \frac{U_j}{H_j}\right)\frac{2}{H_{j-1} + H_j}$$

$$\times\left(1 - \delta_{1j}\right) \qquad (6)$$

and at the bottom:

$$\tau_j^{x,b} = \rho_j A_z\left(\frac{U_j}{H_j} - \frac{U_{j+1}}{H_{j+1}}\right)\frac{2}{H_j + H_{j+1}}\left(1 - \delta_{Nj}\right)$$

$$+ \rho_j R U_j \delta_{Nj} \qquad (7)$$

with equivalent expressions for the y-direction. In these expressions, τ_w denotes a wind stress, δ_{ij} is the Kronecker delta, A_z is a constant vertical turbulent eddy viscosity, and R is a bottom friction coefficient.

In Eqs. (2) and (4) the vertically integrated pressure divided by $g\rho_j$ defines a dynamic height given by:

$$\Phi_j = \gamma\eta - \sum_{i=1}^{j-1}\frac{(\rho_j - \rho_i)}{\rho_j}(H_i - H_{0i}) \qquad (8)$$

where the surface displacement η is given by:

$$\eta = \sum_{i=1}^{N}(H_i - H_{0i}) \qquad (9)$$

and H_{0j} is the thickness of layer j at rest. In order to save computational resources, the surface elevation in Eq. (8) is multiplied by a constant $\gamma \leq 1$ in order

to slow down external gravity waves. For instance, if $\gamma = 1/64$, barotropic gravity waves, including coastal Kelvin waves, will propagate with $1/8$ of their correct speed, while barotropic Rossby waves with wave lengths of 2000 km or less will propagate with 85% to 100% of their correct phase speed. For a typical stratification, baroclinic waves will propagate with an error of 3% or less in phase speed. Slowing down the barotropic waves will increase their interaction with baroclinic modes. However, as long as the speed of propagation of the external gravity wave is kept well separated from that of the internal modes, the effect is insignificant. Details about the gravity wave retardation method are given in Jensen (1996).

The continuity equation becomes:

$$\frac{\partial H_j}{\partial t} + \left(\frac{\partial U_j}{\partial x} + \frac{\partial V_j}{\partial y}\right) = 0 \qquad (10)$$

where it has been assumed that no cross-isopycnal transport takes place.

Discretization is on a C-grid (Arakawa and Lamb, 1977), which is most commonly used for limited area ocean models. The equations are solved using a forward explicit time scheme for the frictional terms and a leapfrog scheme for other terms. The computational mode associated with the leapfrog scheme is removed using a time filter (Asselin, 1972).

3. Open boundary conditions

The open boundary conditions have been divided into three categories: simple conditions, radiation conditions and relaxation schemes. As noted by Røed and Cooper (1986), this distinction is somewhat arbitrary since the simple schemes mathematically are special cases of the radiation schemes. However, since the numerical implementation is different for the stratified case, it is natural to make a distinction between these two groups of OBCs.

3.1. Simple conditions

The simplest condition prescribes the value of a variable along the open boundary. If one indeed can prescribe the exact condition on the boundary consis-

tent with the interior numerical solution, there is not an open boundary problem to be solved. However, in nearly all cases, at least part of the boundary solution is not known a priori, and must be computed. If Φ is the unknown part of any prognostic variable, we define the clamped (CLP) OBC as one that does not change in time:

$$\frac{\partial \Phi}{\partial t} = 0 \tag{11a}$$

This simple condition has been widely used (e.g. Beardsley and Haidvogel, 1981). On a uniform mesh the grid point positions are at $x_i = i\Delta x$, where Δx is the grid spacing. If the boundary is at x_B, the numerical implementation of Eq. (11a) is:

$$\Phi_B^{n+1} = \Phi_B^n \tag{11b}$$

where n refers to the time level.

Nearly as simple is the zero gradient condition:

$$\frac{\partial \Phi}{\partial n} = 0 \tag{12a}$$

where the derivative is taken normal to the open boundary. The numerical implementation for a boundary to the east is simply:

$$\Phi_B^{n+1} = \Phi_{B-1}^{n+1} \tag{12b}$$

where the right hand side is computed from the governing equations. For gravity waves both these conditions are 100% reflective, i.e. the total incident wave energy is reflected (Nitta, 1964). If for instance Φ equals the pressure or a related variable such as a surface elevation or interface displacement, the latter condition gives the same reflection as a wall condition, i.e. $u = 0$, where u is the velocity component normal to the boundary. The reflected wave using the clamped condition has opposite phase of the wave reflected from a wall. So adding or averaging Eqs. (11a) and (12a) leads to an improved condition:

$$\frac{\partial \Phi}{\partial t} + \frac{\partial \Phi}{\partial n} = 0 \tag{13a}$$

which corresponds to radiating out waves with a non-dimensional phase speed of 1. This condition has been discussed in detail by Smith (1974). The numerical form of Eq. (13a) is found by inserting values for the gradient of Φ evaluated at time step $n + 1$, or alternatively, averaging the numerical expressions Eqs. (11b) and (12b):

$$\Phi_B^{n+1} = \frac{1}{2}\left(\Phi_B^n + \Phi_{B-1}^{n+1}\right) \tag{13b}$$

In the test cases, Eqs. (11b), (12b) and (13b) are applied to the layer thickness H_j. Since the harmonic friction terms Eqs. (3) and (5) require grid points outside the actual computational domain, a zero gradient condition involving mirror points is applied to the transport components U_j and V_j, but only for the purpose of calculating this friction.

3.2. Radiation conditions

This class of conditions assume a free wave propagation. Most often normal incidence on the boundary is assumed, so the method can be based on the one-dimensional wave equation:

$$\frac{\partial \Phi}{\partial t} + c_\Phi \frac{\partial \Phi}{\partial x} = 0 \tag{14}$$

where Φ is a field variable for which an OBC is imposed. A review of numerical implementations for two-dimensional flows (oblique incidence) can be found in Hedley and Yau (1988). Orlanski (1976) proposed to calculate the phase speed using finite
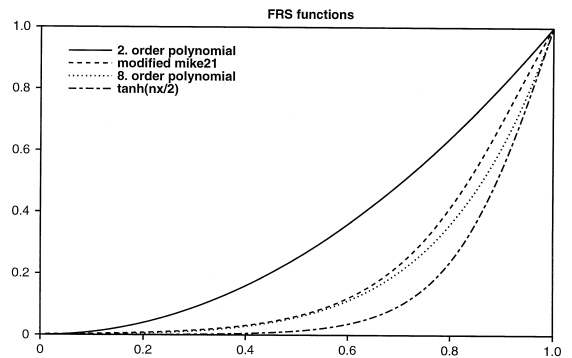

Fig. 2. Relaxation functions varies between 0 and 1 across the relaxation zones. Four typical relaxation functions are shown: the parabolic variation (full line) and the hyperbolic tangent variation (dash–dot line) were used by Martinsen and Engedahl (1987). In the present work, an 8th order polynomial variation (dotted line) was used, following closely the sponge variation used in the MIKE21BW wave model.
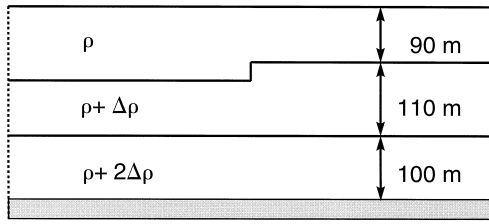
Fig. 3. Vertical cross-section of the initial condition for the internal wave propagation test.

differences. If the open boundary is to the east, a non-dimensional phase speed is computed as:

$$c_\Phi = \max\left\{-\min\left\{\frac{\Phi_{B-1}^n - \Phi_{B-1}^{n-1}}{\Phi_{B-1}^{n-1} - \Phi_{B-2}^{n-1}}, 1\right\}, 0\right\} \qquad (15)$$

Eq. (15) can be put in dimensional form by multiplying by $\Delta x / \Delta t$. Note that negative values (e.g. propagation away from the boundary) of c_Φ are truncated to zero. The boundary value using the Orlanski condition (OL) is calculated as:

$$\Phi_B^{n+1} = c_\Phi \Phi_{B-1}^n + (1 - c_\Phi)\Phi_B^n \qquad (16)$$

The form given by Eqs. (15) and (16) is due to Miller and Thorpe (1981) and is simpler than the original formulation. Camerlengo and O'Brien (1980), (CO), simplified the OL condition by using $c_\Phi = 1$ if $c_\Phi \leq 0$, i.e. only the sign of c_Φ is used. This condition deliberately overestimates the outward propagation speed. An even simpler approach is to choose extrapolation in all cases, i.e. $c_\Phi = 1$. Eq. (16) is traditionally applied to the transport components, i.e. U_j and V_j, rather than the layer thickness H_j, which in this case is computed from the continuity equation Eq. (10).

The evaluation of c_Φ is simple for flows without stratification. For a layered model, a computation layer by layer is a straightforward extension of the two-dimensional case. This strategy will work if a single vertical mode dominates the flow. If two or more vertical modes contribute significantly to the flow simultaneously, a decomposition onto linear vertical modes is, at least in principle, a better

method (Jensen, 1993). For this reason, we have applied the OL and CO conditions to the amplitudes of each vertical mode of the transport components, and after computation of the boundary amplitudes, transformed back to layer formulation. For simplicity, we will assume that the normal mode decomposition is independent of time and space. The normal mode decomposition is shown in detail in Appendix A.

By considering the system of equations as hyperbolic, the method of characteristics may be applied. If we project the linear equations onto vertical normal modes, we simply get a shallow water equation for each vertical mode (e.g. Gill, 1982, pp. 167–175). By solving for the eigenvalues and eigenvectors for each mode, the equations can be written in characteristic form. The derivation is given in Appendix B. For a west (or left) boundary we find:

$$\frac{\partial \tilde{U}}{\partial t} = \frac{1}{2}c^{(k)}\frac{\partial}{\partial x}\left(\tilde{U} - c^{(k)}\tilde{\eta}\right) + U_F \qquad (17)$$

where the tilde indicates a projection on linear vertical modes, $c^{(k)}$ is the phase speed of mode k, and U_F is the sum of the Coriolis term and the frictional terms. For a single layer, Eq. (17) is the same as Hedstrom (1979) condition as tested for a barotropic ocean by Røed and Cooper (1987).

3.3. Relaxation schemes

One alternative to letting disturbances out of the computational domain, is to absorb them in a sponge layer. A good strategy is to use a generalization of this concept, the flow relaxation scheme (FRS), as a frame work in which any open boundary condition may be added (Martinsen and Engedahl, 1987). Since the FRS was developed to impose boundary conditions from a large scale atmospheric model to a fine grid limited area atmospheric model (Davies, 1976, 1983), it is practical to implement a simple data assimilation scheme (e.g. nudging) for the entire model domain. In that respect, prescribing an OBC

Fig. 4. Reference solution for the internal wave radiation test shown as a *x–t* diagram for layer 1 (a), layer (2) (b) and for layer 3 (c). Vectors show the velocity, while contours show layer thickness anomalies in m. The numbers on the horizontal axis indicate grid number. The unit on the vertical time axis is h. Maximum velocity arrows are 0.12 m/s.
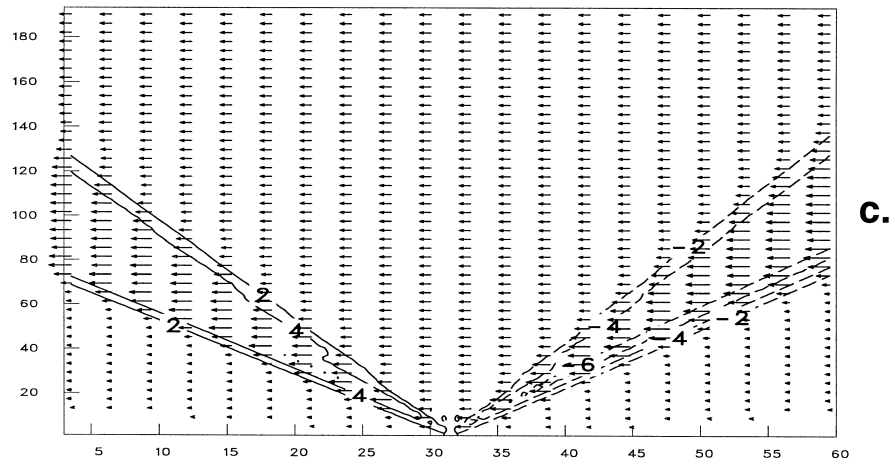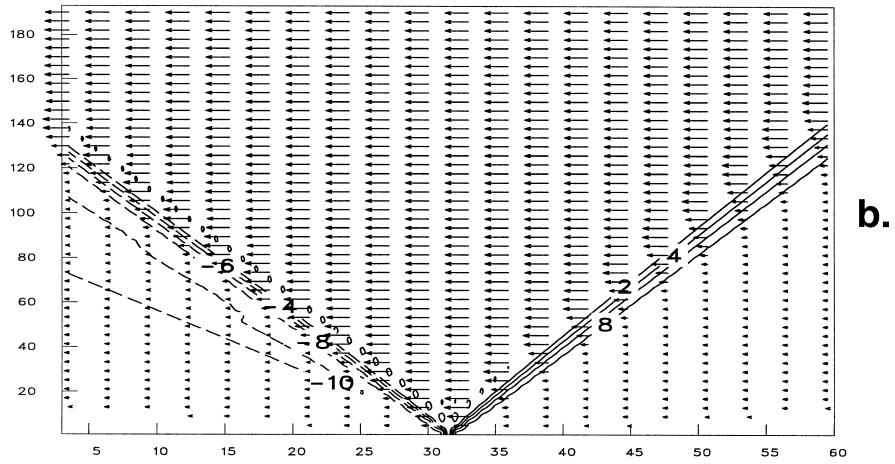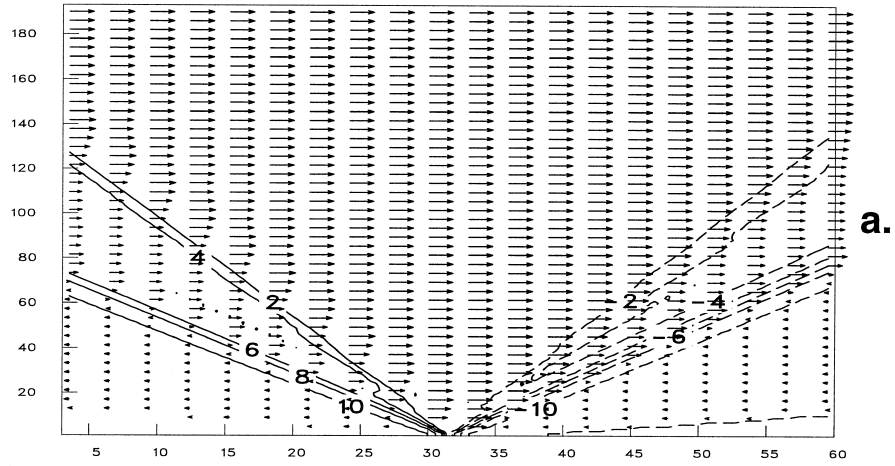
12 cm/s

can be considered a special case of a data assimilation process. The FRS allows specification of the boundary solution for any variable as a sum of an external value, and a value calculated from the interior. The scheme is applied as follows: for any variable the interior solution $\hat{\Phi}$ is calculated. An OBC solution Φ_L is calculated on the open boundary from local interior values. The externally imposed solution on the boundary is Φ_{obs}, where the subscript implies that this value often has been obtained from observations. The boundary solution is then given by:

$$\tilde{\Phi} = \Phi_L + \Phi_{obs} \qquad (18)$$

The FRS technique is now applied as nudging in the vicinity of the open boundary:

$$\Phi = \alpha(x,y,z)\tilde{\Phi} + [1 - \alpha(x,y,z)]\hat{\Phi} \qquad (19)$$

where Φ is the updated solution, which has been relaxed towards the boundary value $\tilde{\Phi}$. The relaxation function α is usually chosen to be 1 on the boundary and decreases to zero in the interior of the domain.

The separation of $\tilde{\Phi}$ into two parts is of course artificial. It simply points out that the solution we relax toward, preferably should be a combination of one that is computed from the interior (by a special method) and one that we wish to prescribe, for instance a forced tidal wave. Note that if Φ is a velocity component and $\tilde{\Phi} = 0$, the FRS zone is reduced to a simple sponge layer.

The optimal width of the relaxation zone and the functional variation within it, depends on the problem. Assume that the relaxation zone extends from $x = 0$ to $x = 1$, with the boundary at $x = 1$. Martinsen and Engedahl (1987) used widths of 3–10 grid points and used the following functions:

$$\alpha(x) = 1 - \tanh\left(\frac{n}{2}(1-x)\right) \qquad (20)$$

and:

$$\alpha(x) = x^2 \qquad (21)$$

where n is the number of grid points in the relaxation zone. The form given by Eq. (20) over a width

of 10 grid points was also used by Cooper and Thompson (1989). In a general purpose code, a more convenient form is:

$$\alpha(x) = [(1-q)x + q]^p \qquad (22)$$

The tanh formulation provides a steeper filter function than a second order polynomial. A similar variation can be obtained using $p = 6$ and $q = 0$ in the polynomial form Eq. (22).

In the Danish Hydraulic Institute Boussinesq wave model (MIKE21BW) the expression used for sponge layers is:

$$\alpha(x) = \left(1 - a^{b^{(1-x)n}}\right)c \qquad (23)$$

with $c = 1$ (Larsen and Darcy, 1983). This form does not equal one for $x = 1$. A polynomial with $p = 8$ and $q = 0.4$ has similar variation in the interval $[0–0.8]$ but goes to one for $x = 1$. Another possibility is to choose $c = a/(a-1)$ in Eq. (23). Fig. 2 shows the variation over the relaxation zone for a few choices of α.

Applying the FRS technique is equivalent to changing the equations in the FRS zone. For a variable Φ, we can write:

$$\frac{\partial \Phi}{\partial t} = f(\Phi) - \frac{\alpha}{\Delta t(1-\alpha)}(\Phi - \tilde{\Phi}) \qquad (24)$$

where the second term on the right hand side is due to the FRS. Note that this corresponds to adding a linear source/or sink term. However, the relaxation coefficient goes to infinity in the edge of the domain, where the calculated solution is replaced by the boundary solution. A finite relaxation factor is obtained using $\alpha < 1$, which corresponds to a larger time constant in the adjustment. One advantage of the form Eq. (24) is that it can be used directly in an implicit scheme.
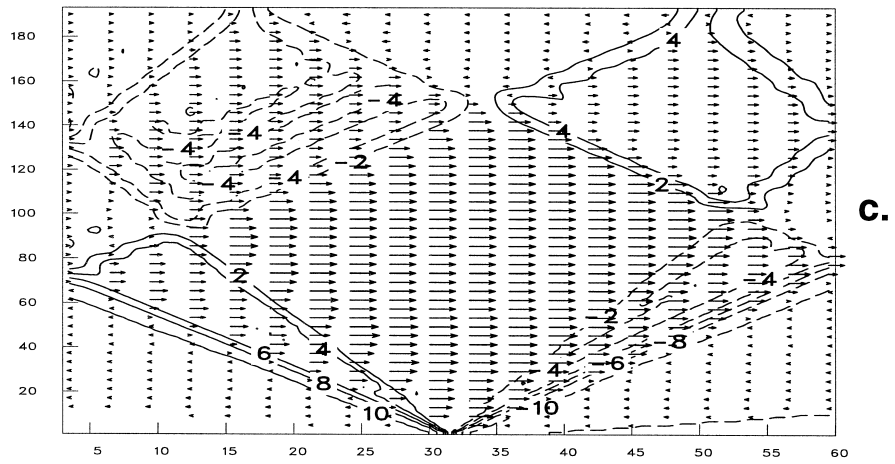
Fig. 5. Contours of layer thickness anomalies and current vectors shown in x–t diagrams for the upper layer using zero gradient (a), clamped (b) and the average of clamped and zero gradient (c). Units are the same as in Fig. 4. Thick arrows indicate velocities in excess of 0.12 m/s.
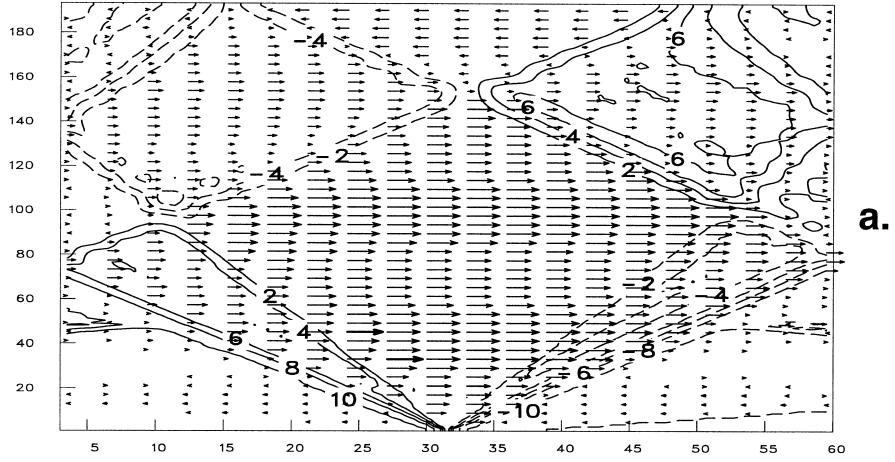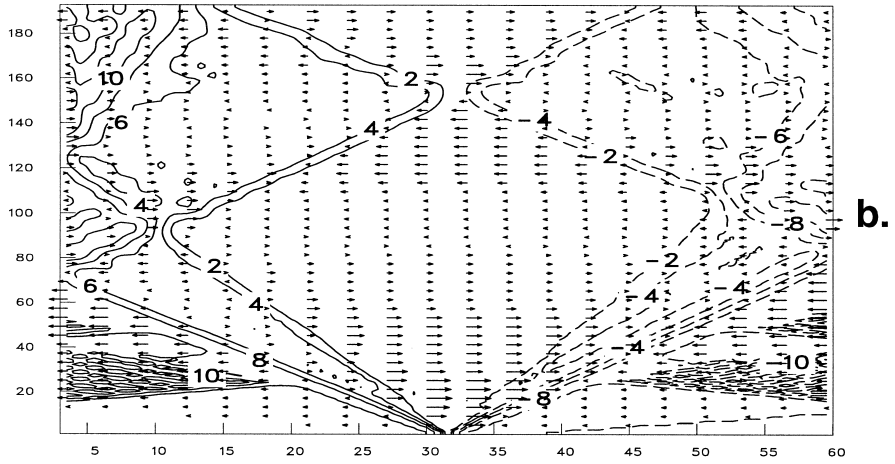
12 cm/s

4. Test problems

The open boundary conditions are tested on three stratified flow problems. The first of these is pure radiation of gravity waves, the second is a simple coastal current and the third is the passage of a storm across a strait. These cases are similar to those investigated by Røed and Cooper (1987).

4.1. One-dimensional internal gravity waves

One of the simplest possible stratified wave propagation problems is that of internal waves in one dimension. Consider an infinitely long channel with a flat bottom. We shall assume that there is no variation in one of the horizontal directions, and that there is no rotation ($f = 0$). This is accomplished by using a single interior grid point in the y-direction and free slip boundary conditions along the walls. We consider a case without external forcing and initially the fluid is at rest with a level surface.

The channel has 3 layers of constant density, each 100 m thick on average, for a total depth of 300 m. The density jump between the layers is constant (1.55 kg/m^3). This depth and stratification results in a long surface gravity wave speed of 54 m/s but is slowed down to 6.6 m/s, when we use $\gamma = 1/64$ in Eq. (8). There are two internal gravity wave modes with phase speeds of 1.25 and 0.70 m/s, respectively. The only stress included is harmonic friction; that is, A_4 is zero, with $A = 300 \text{ m}^2/\text{s}$.

In order to generate waves, there is a discontinuous step of 20 m in the upper layer thickness. This is compensated by the thickness of layer 2, so layer 3 has a constant thickness (Fig. 3). There are no pressure gradients in layer 1 initially, since the surface is level. In layers 2 and 3 there is a horizontal pressure discontinuity (high pressure to the right in Fig. 3), which accelerates the flow in the direction of low pressure.

A grid spacing of 11 km was chosen and the model was integrated for 8 days with a time step of 600 s. A reference solution was obtained in a domain so wide (i.e. > 7000 km) that reflections cannot return from the boundaries to the central part of the domain during the time of integration.

Fig. 4 shows the reference solution in a $x–t$ diagram for a subdomain which contains the 30 grid

points (330 km) in the center, where only waves propagating away from the discontinuity exist. A surface wave is generated by the pressure discontinuity and causes the surface to rise on the left and fall on the right side of the discontinuity. These surface fronts propagate away with the external gravity wave speed and leaves a weak barotropic current flowing from right to left in Figs. 3 and 4.

Let us consider a location away from the discontinuity. After passage of the first baroclinic mode, an upper layer flow to the right, which nearly compensates the deep flow in layer 3, is established. The thickness of layer 2 is nearly constant and the flow is weak in that layer, until the front associated with the second vertical mode passes. A projection of the solution on vertical modes (see Lighthill, 1969) also reveals a very small amplitude of the first vertical mode in layer 2. After passage of the second vertical mode, all available potential energy has been converted into kinetic energy: a steady baroclinic current is left behind. The upper layer transport (left to right) is nearly, but not quite, compensating the transport in layers 2 and 3. The maximum current is 0.1 m/s and is found in layer 1. A similar example of wave adjustments in a stratified fluid can be found in Gill (1982, p. 164).

For the test of OBCs we use a smaller domain, where the artificial boundary is placed 30 grid points away from the pressure discontinuity. An excellent open boundary condition should give a solution nearly identical to that in Fig. 4. In ocean models, the simplest solution is to place a vertical wall at the boundary. Fig. 5a shows the result for that case. The external mode contaminates the solution everywhere after about 20 h. The first baroclinic mode reflects after 80 h and severely distorts the solution in the domain as it propagates back towards the center of the basin. This closed wall boundary condition can be considered the ''reference worst case'' scenario for the present problem. Some open boundary conditions are not necessarily better. In fact, the zero gradient condition Eqs. (12a) and (12b) gives exactly the same solution as the wall for this case.

Poor choices in open boundary conditions can be worse than a wall: Fig. 5b shows the results using the clamped condition Eqs. (11a) and (11b), where the thickness of each layer is held at its initial value along the open boundaries. Currents up to 0.36 m/s
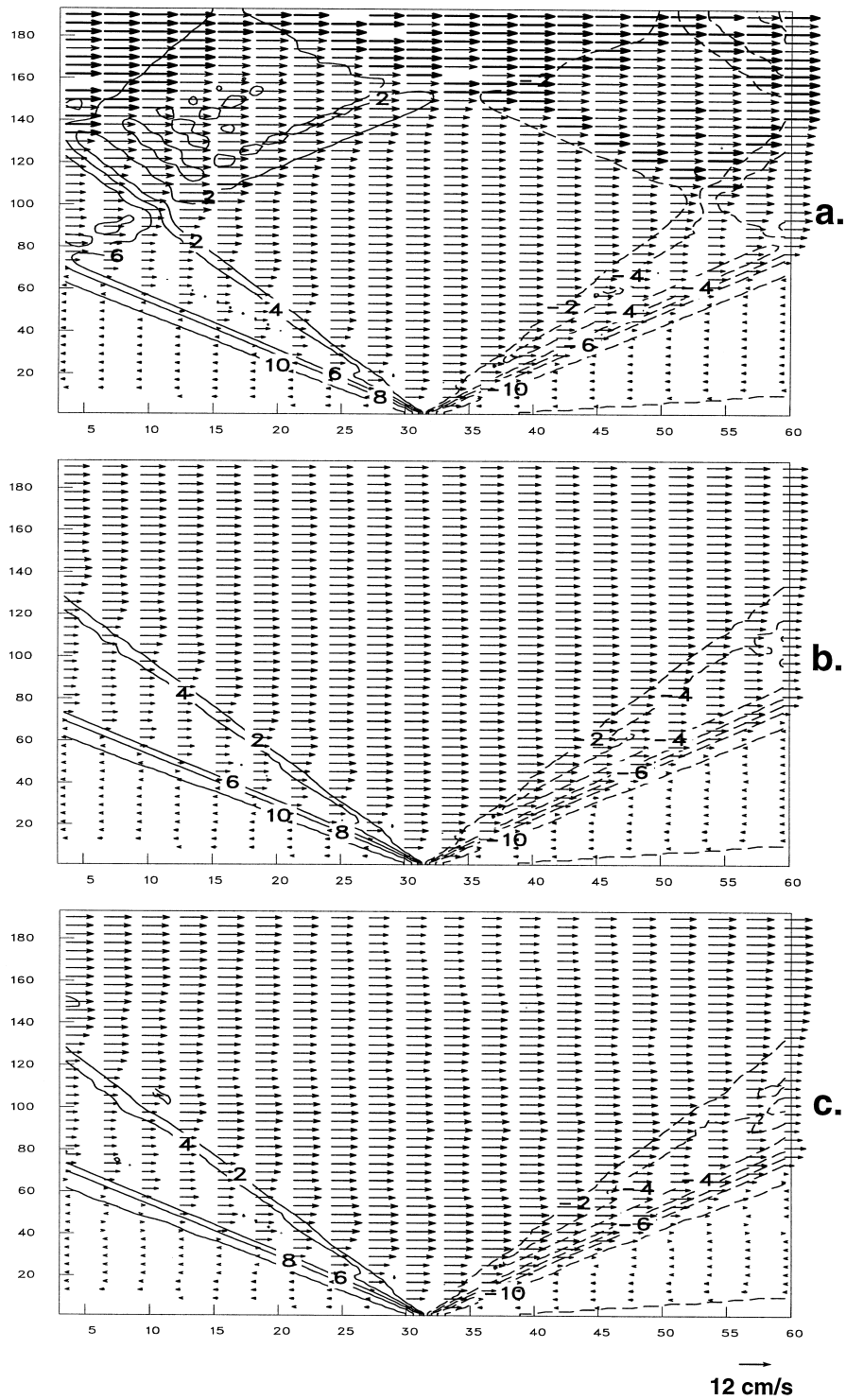
Fig. 6. As Fig. 5, but for the Camerlengo–O'Brien OBC (a), the Orlanski OBC (b) and the method of characteristics (c).

are found in the two lower layers because the pressure difference between right and left edge in Fig. 3 is held constant. However, this condition does allow inflow and outflow past the artificial boundaries and note that the thickness anomaly of the reflected wave has the opposite sign as that of the wave reflected from a wall.

Condition Eqs. (13a) and (13b), which corresponds to selecting the average of the zero gradient and the clamped condition shows a solution slightly better than the wall solution: the external mode has been removed (Fig. 5c). In an explicit model, the time step is chosen so that the Courant number is just below one in order to minimize the computational effort. Consequently, the fast external wave propagation satisfies the radiation condition Eq. (14). Not surprisingly, the extrapolation condition Eq. (16) with $c_\Phi = 1$ gives us exactly the same result.

Figs. 6 and 7 show solutions using selected radiation conditions. The formulation by Camerlengo and O'Brien (1980) (CO) removes the external mode, but is weakly unstable and cause an acceleration of the flow (Fig. 6a). This weak instability is easily removed by occasional smoothing along the open boundaries, but reflections still occur. The solution in Fig. 6a was obtained without a filter, but for longer integrations a Hanning filter (a binomial 1–2–1 filter), applied every 10 time steps, is sufficient to remove this instability. The filter is only applied in the direction perpendicular to the boundary over the nearest 3 rows of grid points closest to the open boundary. Smoothing every time step (or over additional rows of grid points) adds excessive diffusion along the boundary.

The Orlanski (OL) condition (Fig. 6b) based on the normal mode decomposition from Appendix A

works nearly perfectly. However, for this particular problem, a natural separation of modes occurs, and computing the phase speeds from Eq. (15) layer by layer works almost as well.

The method of characteristics (Fig. 6c) is nearly as good as OL. However, note that the current in the center of the domain is not steady due to weak reflections. In layer 2 (not shown) these reflections are more noticeable.

Fig. 7a shows the best results obtained with a 10 grid points wide sponge. Velocities were relaxed toward zero using $p = 4$ and $q = 0$ in Eq. (22). The thicknesses of the layers were computed from continuity Eq. (10). A wider sponge will reduce the magnitude of the reflections, but also increase computational costs.

When applying the FRS it is important to relax toward the correct solution. This is clearly demonstrated in Fig. 7b, where the solution was relaxed toward horizontal isopycnals. This is the correct solution after the fronts associated with three vertical modes have passed. However, the velocities were relaxed toward zero, which is the correct initial condition. Relaxing toward the initial condition for both velocity and layer thickness in each layer gives excellent results (Fig. 7c). Similarly, relaxing toward constant thickness of each layer will work if the correct velocities after the frontal passage could be specified. For the solutions in Fig. 7b,c a 10-point wide relaxation zone was used on each side and $p = 8$ and $q = 0.4$ was used in Eq. (22). With a 5 grid points wide FRS zone, the results were still good, with reflections similar to those seen for the CHA method.

The best OBC for this case is OL based on a normal mode decomposition. A close second best is

Fig. 7. As Fig. 5, but using a 4th order polynomial sponge condition on the velocity components (a), FRS relaxing towards zero for velocities and zero layer thickness anomaly (b) and FRS relaxing towards the initial condition (c). The 10-point wide sponges or relaxation zones on each side of the domain of interest are not shown in the plots.

Fig. 8. Reference solution for a coastal jet at day 20 using periodic boundary conditions for layers 1–3 ((a)–(c)) in the east–west direction. Along the northern boundary, the clamped condition is used. Contours show layer thickness anomalies in meters, while the vectors show currents. Contour intervals are 10 m (a) and (b) or 5 m (c). Maximum velocity vector is 0.4 m/s. Numbers along each axis refer to grid points.

Fig. 9. Contours of layer 1 thickness anomalies and current vectors for the coastal jet problem at day 20 using walls at the eastern and western boundary (a), the clamped OBC (b) and the Orlanski condition (c). Contour intervals are 5 m (a) and (b) or 10 m (c). Maximum velocity vector is 0.4 m/s. Thick arrows indicate velocities larger than 0.4 m/s. Numbers along each axis refer to grid points.
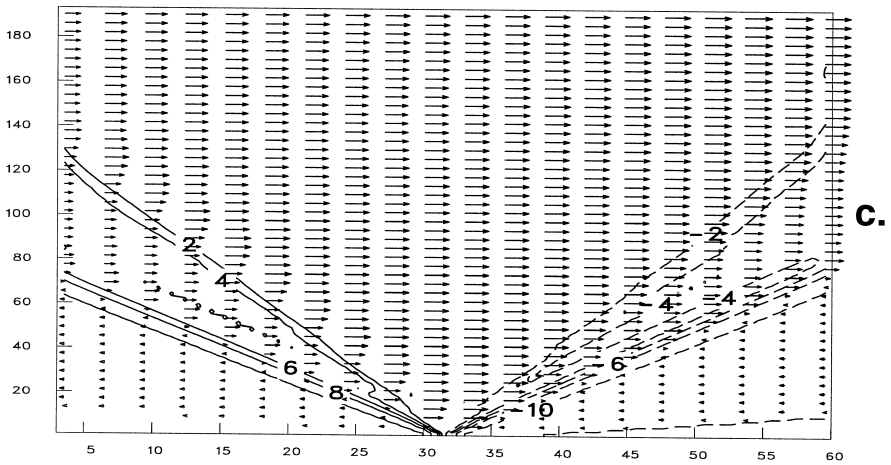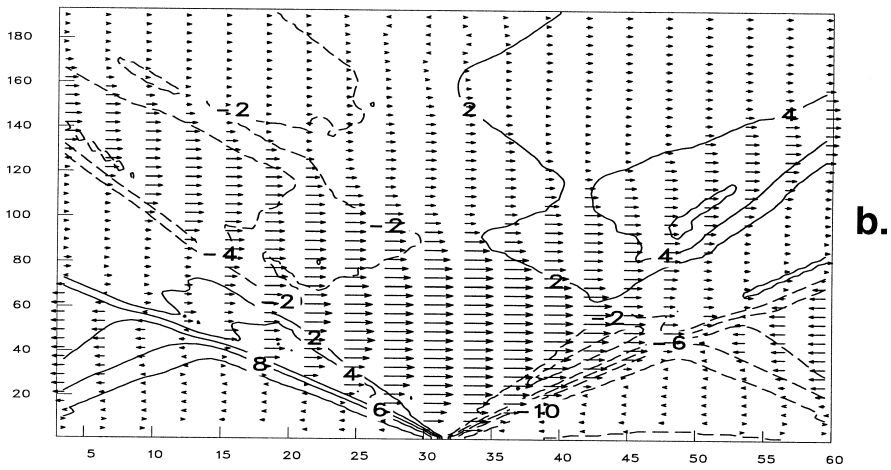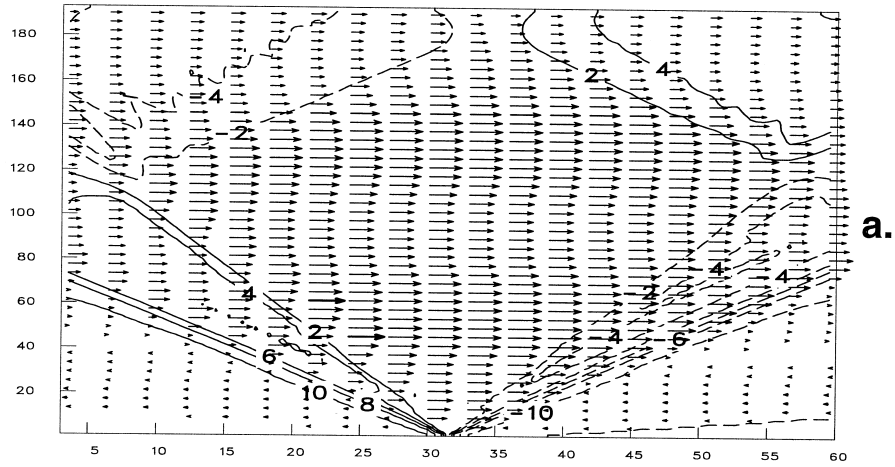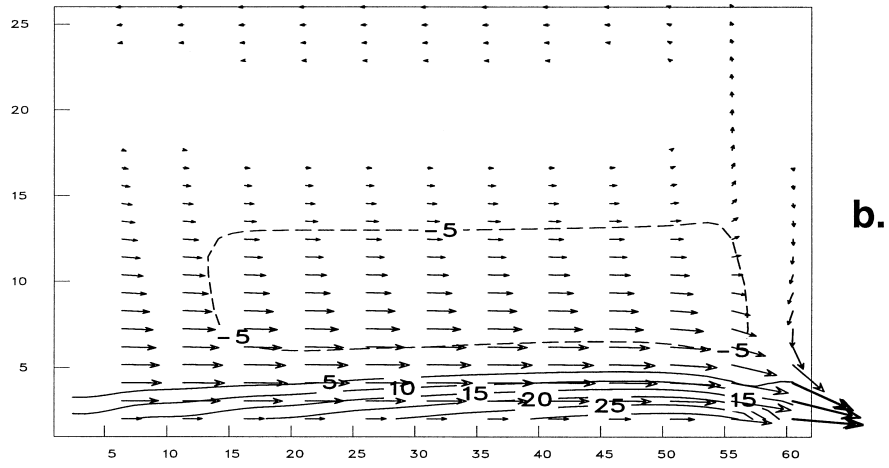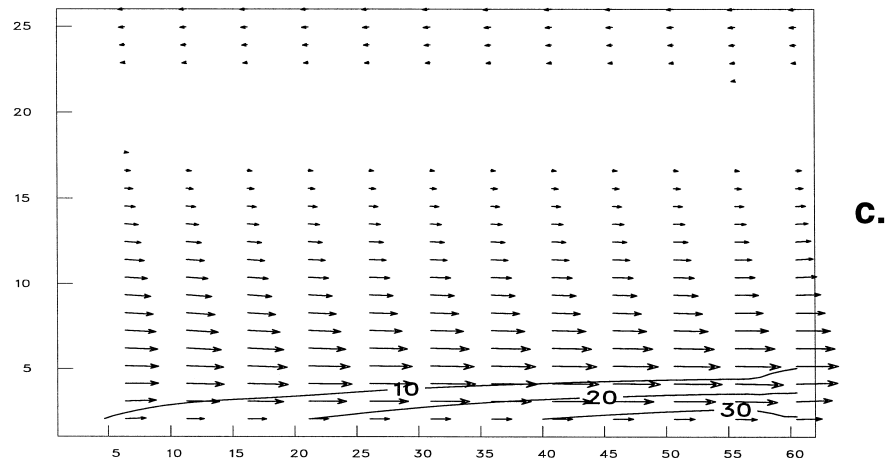
12 cm/s
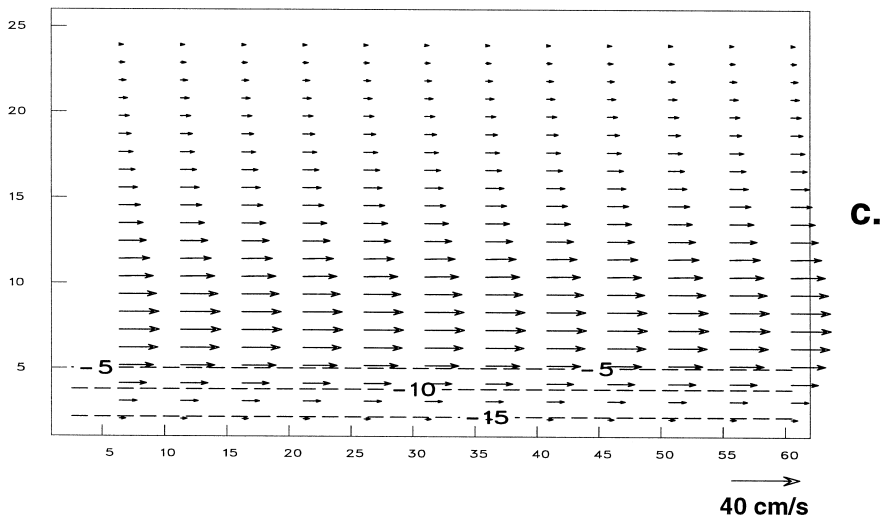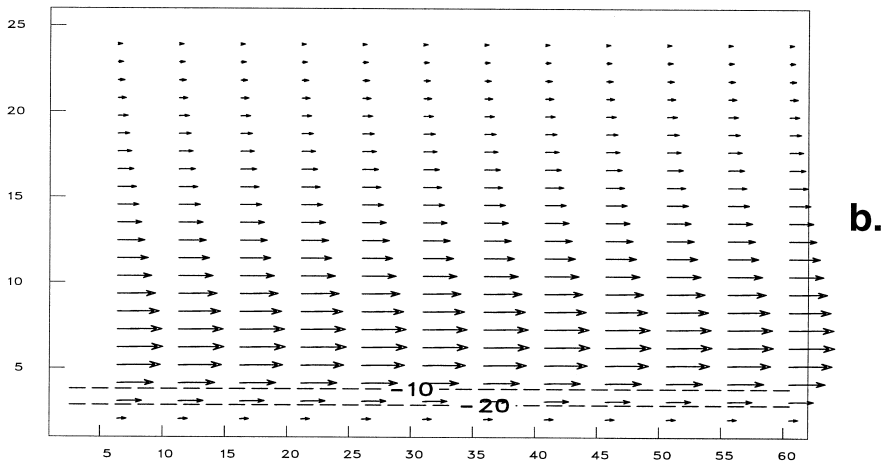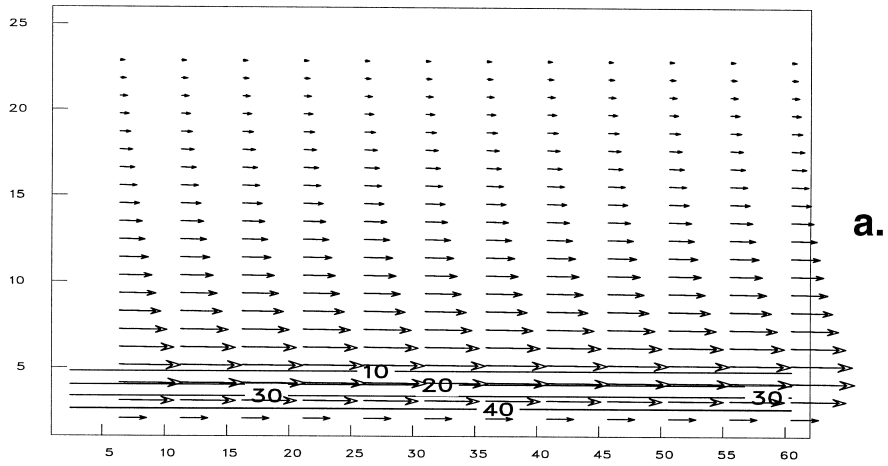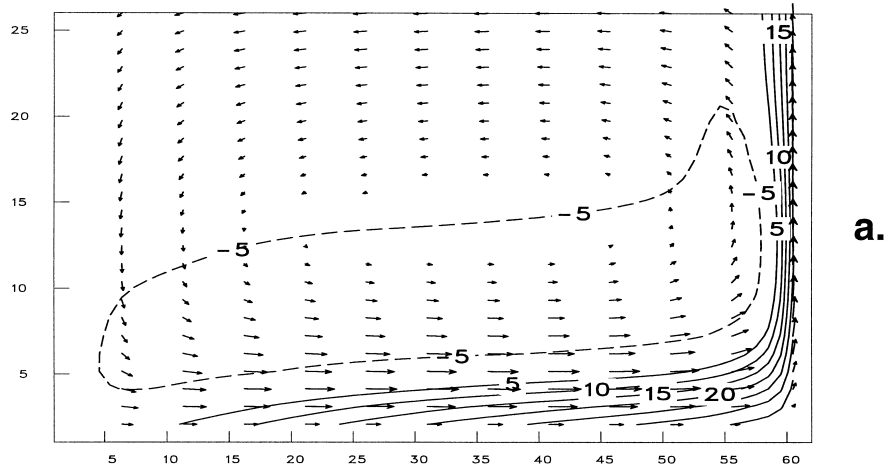
40 cm/s

the FRS using a 10-point relaxation zone and the third best performance was obtained by the method of characteristics (CHA) using normal modes.

4.2. Coastal current

We consider a rectangular ocean with a straight coast to the south. We use a *f*-plane at 24.5°N and a domain which is 660 km wide in the alongshore direction and extends 330 km into the ocean from the coastline. The initial thickness of each layer is 100 m with the same densities as in the previous case, and the sea is at rest. The forcing, which is applied instantaneously, is an eastward alongshore wind which varies offshore as:

$$\tau_w^x = \tau_0 \exp(-y/L) \tag{25}$$

where $L = 132$ km sets the e-folding scale and the magnitude of the wind stress is given by $\tau_0 = 0.1$ N/m^2. Along the coast we apply the no-slip boundary condition ($U_j = V_j = 0$) for all layers. In order to adequately resolve the boundary layer along the coast, a constant harmonic friction coefficient of 400 m^2/s was used, while other stresses were set to zero. The horizontal grid spacing was 11 km in both directions and a value of $\gamma = 1/16$ slowed the barotropic gravity wave phase speed down to 13.2 m/s, which allowed a time step of 100 s.

Along the northern boundary the thicknesses of all layers are held fixed (CLP OBC) as suggested by Røed and Cooper (1986) for a similar test case. In this problem there is no variation in the alongshore direction, so we use periodic boundary conditions at the cross-shore boundaries on the layer thickness and transports for the reference solution (Fig. 8). The model is integrated for 20 days. The Ekman transport is towards the coast, which increases the upper layer thickness and sets up alongshore velocities in a few days. Layers 2 and 3 have negative thickness anomalies along the coast. An eastward geostrophic transport exists in the boundary layer near the coast. The transport in each layer is accelerating linearly in time

if friction is absent (e.g. see Csanady, 1982, pp. 75–91 for a discussion of analytical solutions). At day 20, the maximum alongshore velocities in layers 1, 2 and 3 are 0.37, 0.27 and 0.23 m/s, respectively.

For this problem we find, not surprisingly, that the zero gradient condition works perfectly. To machine precision we get the same solution as for periodic boundary conditions. Another simple solution is to place walls at the ends. A north–south jet along the eastern wall lets some fluid out of the northern clamped boundary, but a substantial cyclonic recirculation is present (Fig. 9a). In contrast, using clamped boundary conditions along all boundaries, results in a strong outflow on the eastern boundary (Fig. 9b). The numerical solution is subject to a weak instability, which can be removed by decreasing the time step to 60 s and by spatial smoothing along the outflow boundary. The Hanning filter described in Section 4.1, but applied only every 100 time steps in the direction perpendicular to the boundary and every 20 time steps in the direction parallel to the boundary, is sufficient to make the computation stable. Applying the filter to both open boundaries, and more frequently in the direction perpendicular to these, improves the solution further. The reason is that such a filter indirectly imposes a zero gradient condition rather than a pure CLP condition.

The simplest method based on radiation conditions, the extrapolation condition and the sum of the clamped and the zero gradient condition also works extremely well for this simple case. However, the cases where the wave speed is computed numerically do poorly. Since there is only acceleration of currents it is not surprising that methods based on wave propagation fail. Fig. 9c shows the best of these schemes, which was OL based on normal modes. Currents are underestimated and a weak recirculation is seen in the northern part of the domain. Using the more efficient CO scheme with a layer by layer approach, only degraded the solution in Fig. 9c slightly.

Fig. 10. As Fig. 9, but for the characteristic boundary condition (a), the FRS used as a sponge (b) and FRS relaxed towards the solution at the center of the basin (c). In (b) and (c) the 10-point wide sponges or relaxation zones on each side of the domain are not shown on the plots. Contour intervals are 5 m (a) and (b) or 10 m (c).
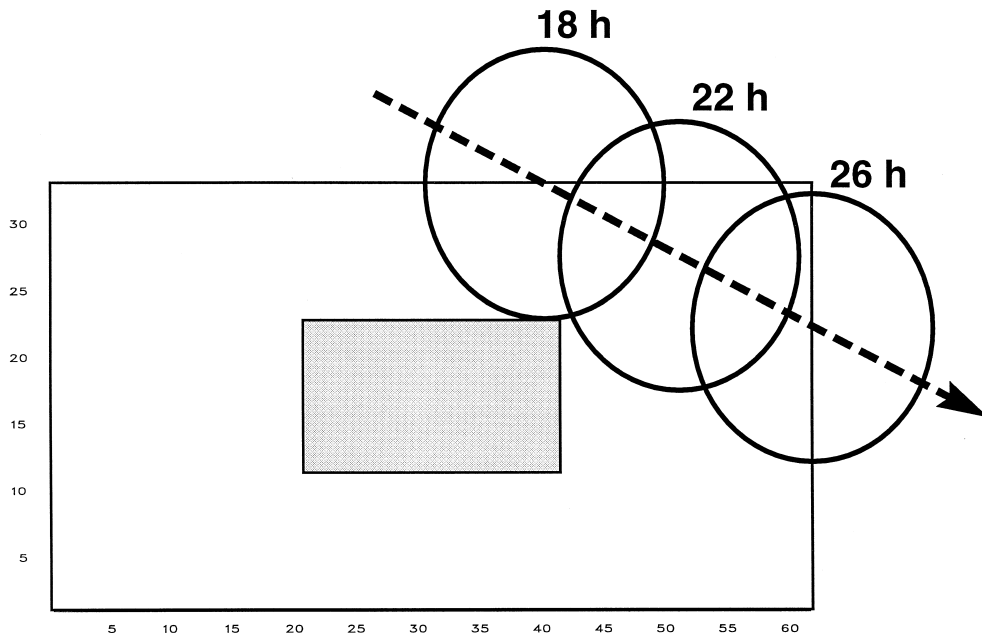
a.

b.

c.

40 cm/s
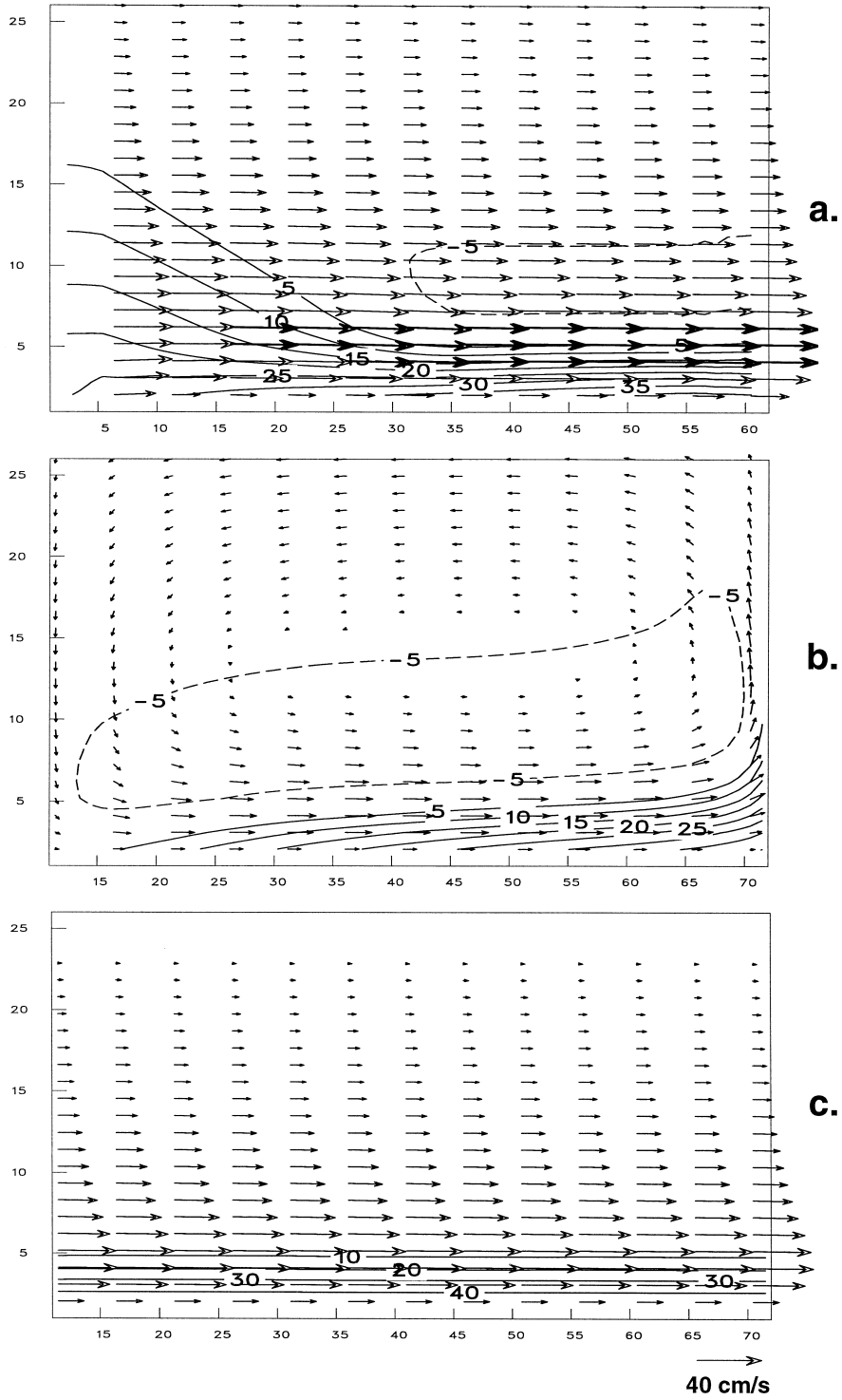
Fig. 11. Model domain for storm case. The shaded area shows the position of a bank, which reduces the depth from 300 m to a minimum of 220 m. The storm track is shown by the dashed line. The circles show the position of maximum winds at 18, 22 and 26 h, respectively. Numbers along each axis refer to grid points.

The method of characteristics (Fig. 10a) does not induce any artificial recirculation, but overestimates the maximum current velocities by 24% in the surface layer and more than 50% in the bottom layer. The method is also sensitive to the normal mode decomposition. For example, if we use the identity matrix, which corresponds to apply Eq. (B.19) to each layer, currents are strongly underestimated and a fairly strong recirculation occurs in all layers. In that case the solution is similar to that in Fig. 10b, which shows the upper layer solution when the FRS is used as a simple 10-point wide sponge. One way to improve on the FRS solution is to relax towards a ''correct'' solution. For instance, relaxation towards the solution at the previous time step along a cross-section taken at the center of the domain works very well (Fig. 10c). However, the cumulative effect of relaxing towards a previous time step, slows down
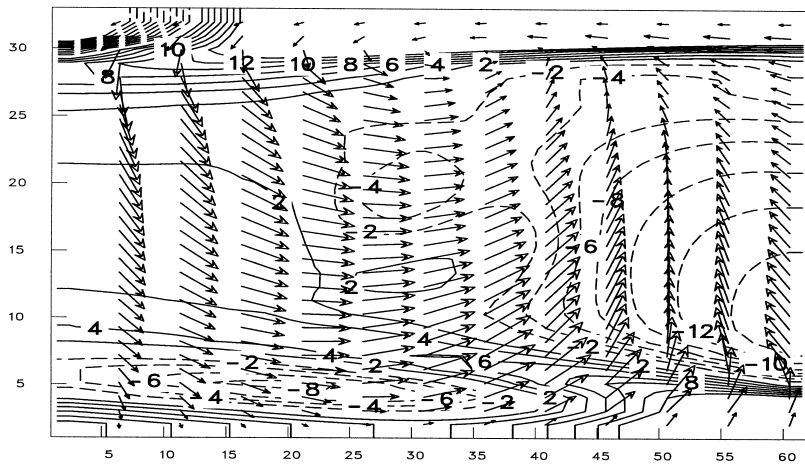
the currents slightly compared to the reference solution.

For this test case, GRA is perfect. Schemes based on extrapolation, i.e. Eqs. (13a), (13b) and (16) with $c_\phi = 1$ also work well. The CHA scheme is acceptable, while FRS requires a reasonably correct boundary solution.

4.3. Storm over a strait

This is a more realistic case with a cyclonic storm crossing an infinitely long strait or channel. The width of the strait is 330 km and we want to model a 660 km wide section using OBCs. Bottom topography in terms of a double cosine shaped subsurface bank is present in the lowest layer (Fig. 11). The maximum height above the sea bed is 80 m and the horizontal dimensions of the depth anomaly are 240
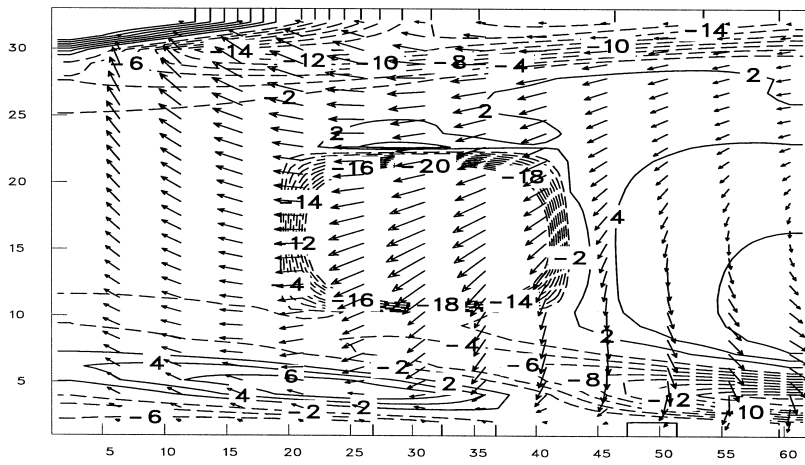
Fig. 12. Reference solution of the flow at 48 h for the storm case. Contours show the layer thickness anomaly with 2 m interval and the vectors show the velocity for layers 1–3 ((a)–(c)). In layer 3, only contours down to -20 m are shown over the shallow topographic feature. Maximum velocity arrows are 0.9 m/s. Numbers along each axis refer to grid points.
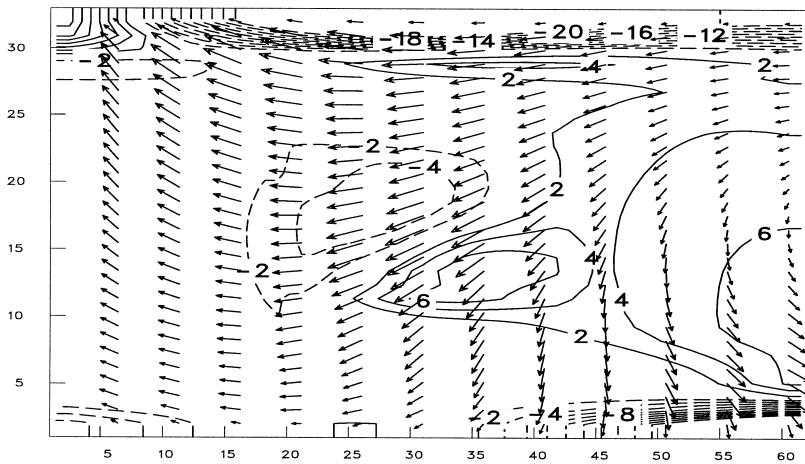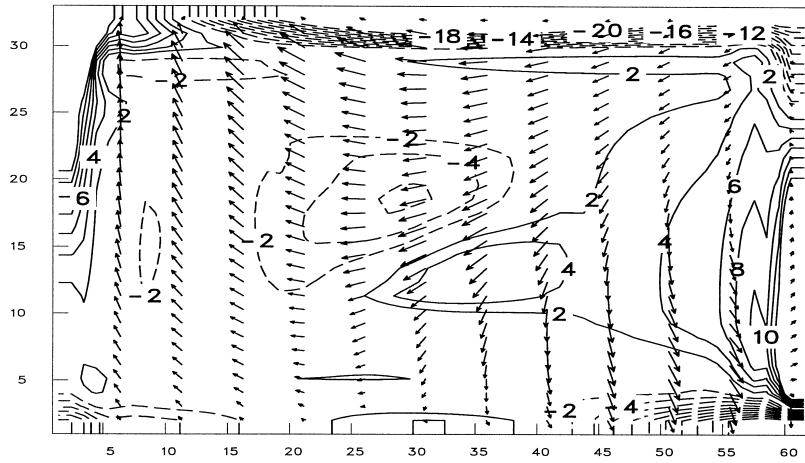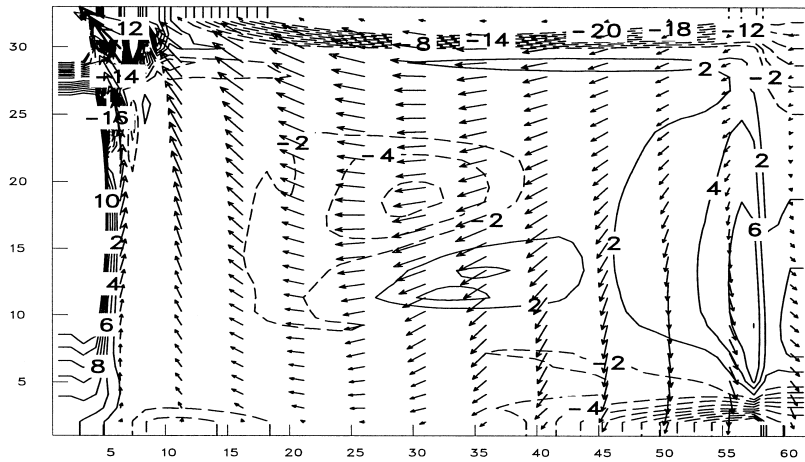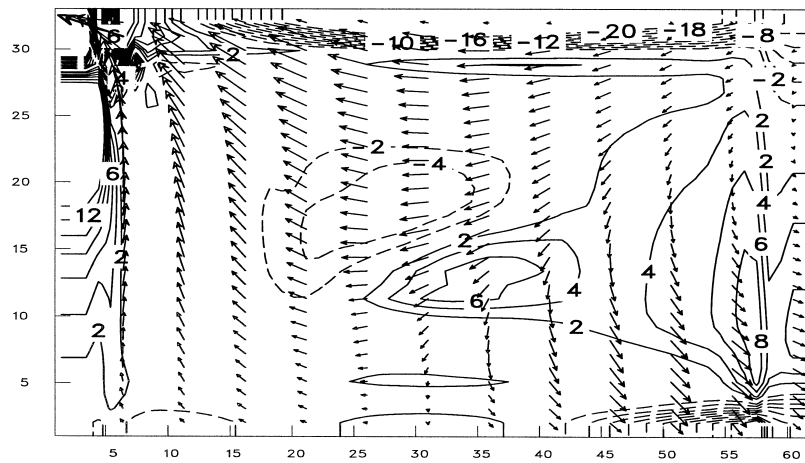
a.

b.

c.

90 cm/s

by 120 km. Along the northern and southern coast-lines the no-slip boundary condition is applied as in the previous case. Biharmonic diffusion is applied, subject to the additional boundary condition:

$$\nabla^2 \left(\frac{U_j}{H_j} \right) = 0 \qquad (26)$$

The lateral diffusivities for momentum are $A = 100$ m^2/s and $A_4 = 10^{11}$ m^4/s, while the vertical turbulent eddy viscosity coefficient was $A_z = 10^{-3}$ m^2/s. A bottom friction coefficient $R = 10^{-6}$ s^{-1} was used. The resolution and the time step are the same as in the previous case.

The storm is moving in from the west-northwest with a speed of 11 m/s over the northeastern part of the channel, and is crossing the open boundary, so that we have the case of strong forcing at the edge of our domain. Maximum wind stress of 2.0 N/m^2 occurs 200 km from the center of the storm. The storm track is shown in Fig. 11, with storm positions at 18, 22 and 26 h. The circumference of the storm shows where winds are at the maximum. The model was integrated for 48 h.

Fig. 12 shows the reference solution for all 3 layers. This solution was obtained by extending the length of the model domain to 1980 km and applying different OBCs. It was verified that the solution in the central third part of the extended domain did not depend on the OBCs during the first 48 h. For the truncated domain (Fig. 11), there is strong forcing outside the domain, preventing us from getting the same solution as the reference even with a perfect OBC.

Given the difficulties with the simple tests above, one might expect even worse results here. However, away from the boundaries, all runs are in fact reasonable for the upper layer. This is due to the strong direct local response to the wind. Maximum currents are about 0.9 m/s in the upper 100 m. Coastal Kelvin waves are generated and propagate along the

northern and southern boundaries. A solution with acceptable OBCs should not have any Kelvin waves propagating along the eastern or western boundaries. Fig. 13 shows results from layer 2 using a wall (a), CLP (b) and the GRA condition (c), while Fig. 14 shows the results from applying CO (a), CHA (b) and FRS with 10-point wide relaxation zones (c). It is noteworthy, that the circulation in the clamped and zero gradient solutions are as unrealistic as for the wall condition. The CHA solution has Kelvin wave propagation along the eastern boundary, but is otherwise acceptable. The CO solution is marginally better than the OL solution (not shown), while the FRS solution is closest to the reference.

5. Summary and discussion

The most commonly used open boundary conditions were presented in Section 3. These were the clamped and zero gradient as well as a number of one-dimensional radiation conditions. The method of characteristics based on linear equations was presented as a more complete alternative to let gravity waves out of the computational domain. The philosophy in the flow relaxation scheme (FRS) is to relax the interior solution in the vicinity of the boundary to an external "correct" solution. When used as an OBC the FRS is in essence a generalized sponge in the sense that the difference between the interior solution and the "correct" solution is relaxed to zero.

Three test cases were presented in Section 4. The simple one-dimensional wave radiation problem for a 3-layer fluid proved to be a fairly stringent test for many OBCs. Only the Orlanski condition applied to a normal mode decomposition of the flow and the FRS solution gave excellent results. The method of characteristics is acceptable for this problem, while other methods clearly give inferior results. In particu-

Fig. 13. Layer thickness anomaly and current vectors for layer 2 for a wall boundary condition (a), the clamped condition (b) and zero gradient (c). Contour interval is 2 m. Compare with the reference solution in Fig. 10b. Maximum velocity vector is 0.9 m/s. Numbers along each axis refer to grid points.
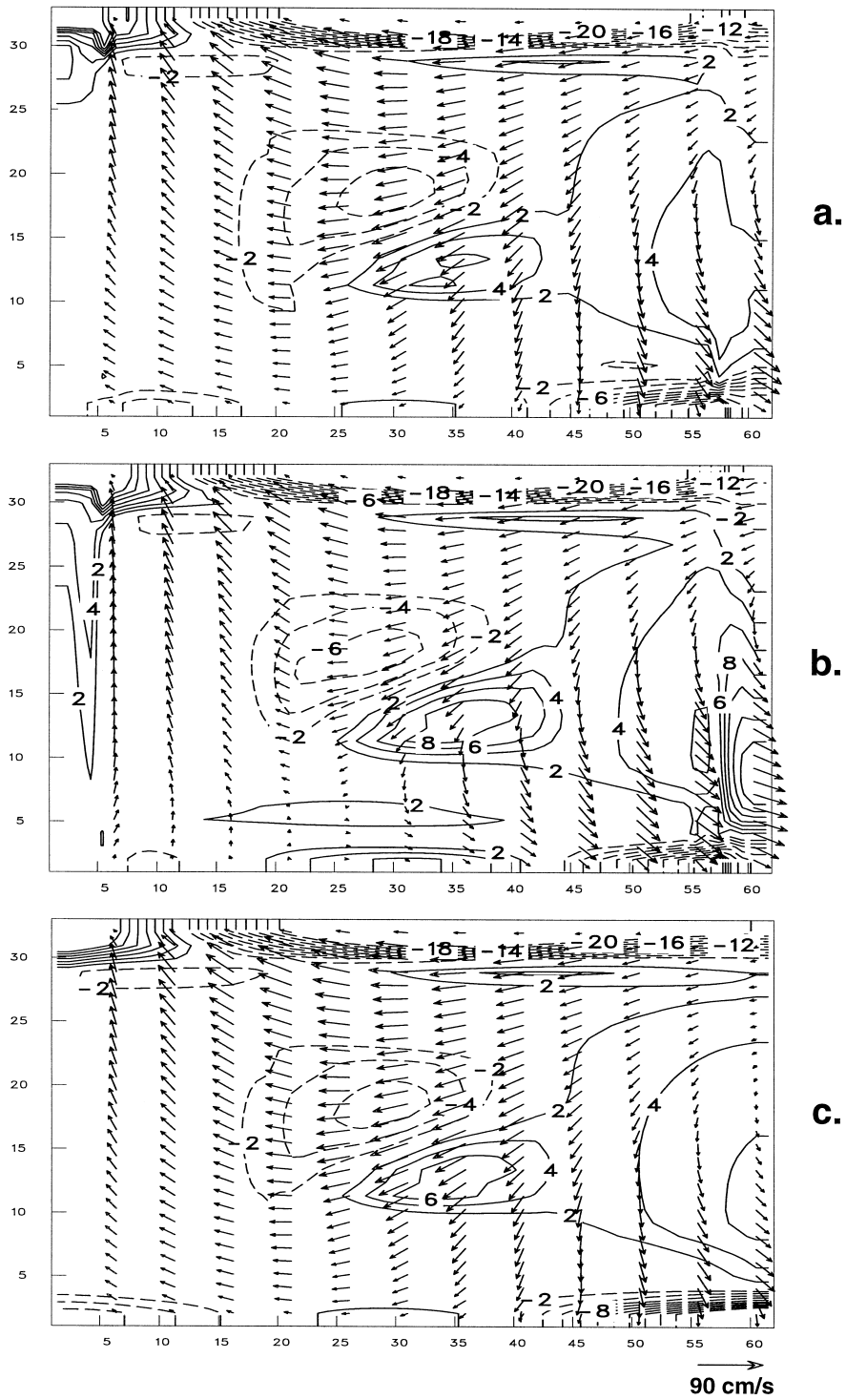
Fig. 14. As Fig. 13, but for the Camerlengo–O'Brien condition (a), method of characteristics (b) and the FRS (c). The 10-point wide FRS zones are not shown in (c).

lar, one gets full reflection from the zero gradient method and the clamped OBC.

For a steady coastal jet, several methods performed very well. Best was the zero gradient method, followed closely by the extrapolation method and the sum of the zero gradient and clamped method. Methods where the phase speed was computed numerically had problems since wave propagation does not play a role in the correct solution. The method of characteristics was better than other schemes based on the hyperbolic form of the equations, but far from perfect. The FRS worked only well when relaxed towards a reasonably correct solution. This, of course, presents a problem applying this method in general.

The realistic case of a storm crossing a strait had time-dependent circulation as well as wave generation. Worst performance was seen for the clamped and zero gradient conditions. Acceptable results were obtained with the method of characteristics, while excellent results were found using Orlanski, Camerlengo–O'Brien and the FRS. It should be noted that increasing the width of the FRS zones improves the solution in all of the test cases. Using 5 grid points or less in the relaxation zones gave less satisfactory performance than cases where 10 points were used. However, increasing the width of the FRS zones from 10 to 20 grid points did not improve the results significantly. For the barotropic models, Martinsen and Engedahl (1987) also concluded that the performance gets better when increasing the width of the relaxation zones.

The actual numerical implementation does play a role in the results presented here. More complicated schemes such as the method of characteristics can be computed in different ways on the grid and some experimentation with the choices showed that it did influence the performance. Similarly, some smoothing along the boundaries is required for the radiation conditions. Too much smoothing will degrade the performance, while too little may result in numerical instability.

The most important conclusion in Røed and Cooper (1987) was that any single OBC scheme did not prove to be the best in all test cases. This conclusion can also be made from this study. In the Røed and Cooper (1987) study of barotropic models, the scheme based on the method of characteristics performed better than the others in general. In our case, where a projection on vertical normal modes from a reference basic state was used, this method was less successful. Computing time- and space-dependent normal modes might improve the method. However, even in the time- and space-independent, linearized form used here, the CHA method requires much larger computational efforts than the simple schemes.

In terms of robustness, the FRS is superior to other schemes and is recommended for general use. Our results suggest that the width of the relaxation zones should be in the range of 5 to 10 grid points. However, it is extremely important to emphasize that knowledge of a reasonably correct solution is required. The scheme has the advantage that it can be generalized to include forcing and combine a sponge with any radiation condition (Martinsen and Engedahl, 1987). The sponge will tend to absorb weak reflections from an imperfect approximation to the characteristics, so a fairly simple radiation condition may be sufficient.

Acknowledgements

Appendix A. Vertical normal modes

In order to apply radiation conditions for each mode separately, we project the solution on vertical normal modes. For simplicity we assume $\partial/\partial y = 0$ in the derivation that follows. We simplify the model equations Eqs. (2)–(10) to the linear shallow water

equations. In absence of friction, these can be written:

$$\frac{\partial U_j}{\partial t} - fV_j = -gH_{0j}\frac{\partial \Phi_j}{\partial x} \tag{A.1}$$

$$\frac{\partial V_j}{\partial t} + fU_j = 0 \tag{A.2}$$

$$\Phi_j = \gamma \sum_{i=1}^{N} (H_i - H_{0i}) - \sum_{i=1}^{j-1} \frac{(\rho_j - \rho_i)}{\rho_j}(H_i - H_{0i}) \tag{A.3}$$

$$\frac{\partial H_j}{\partial t} = -\frac{\partial U_j}{\partial x} \tag{A.4}$$

where the notation is the same as in Section 2.

We follow the derivation by Lighthill (1969). Partial differentiation of Eq. (A.1) with respect to time t and using Eq. (A.2) gives:

$$\frac{\partial^2 U_j}{\partial t^2} + f^2 U_j = -gH_{0j}\frac{\partial^2 \Phi_j}{\partial x\partial t} \tag{A.5}$$

Eliminating H_j using Eq. (A.3) yields:

$$\left(\frac{\partial^2}{\partial t^2} + f^2\right)U_j = g\mathbf{A}\frac{\partial^2 U_i}{\partial x^2} \tag{A.6}$$

where the $N \times N$ matrix $\mathbf{A}$ has the elements given by:

$$a_{ji} = \left(\gamma - \frac{\rho_j - \rho_{\min(j,i)}}{\rho_j}\right)H_{0j} \tag{A.7}$$

Plane wave solutions of the form $U_j = \mathscr{U}_j\exp[-i(\kappa x - \omega t)]$ must satisfy the relation:

$$(\omega^2 - f^2)\mathscr{U}_j = g\kappa^2 a_{ji}\mathscr{U}_i \tag{A.8}$$

where ω is the angular frequency, κ is the wavenumber, and $\mathscr{U}_j$ is an amplitude.

We can expand on vertical normal modes by writing:

$$U_j = \sum_{k=1}^{N} \alpha_{jk}\tilde{U}_k \tag{A.9}$$

where α_{jk} is component j of eigenvector k of the matrix $\mathbf{A}$. The normal mode amplitudes are computed from:

$$\tilde{U}_k = (\alpha_{j\kappa})^{-1}U_j \tag{A.10}$$

where $(\alpha_{jk})^{-1}$ denotes the inverse of matrix α_{jk}. For free waves, the dispersion relation is from Eqs. (A.8) and (A.10):

$$\omega^2 - f^2 - gh^{(n)}k^2 = 0 \tag{A.11}$$

where $h^{(n)}$ is the equivalent depth, i.e. an eigenvalue to $\mathbf{A}$.

Along an open boundary, we compute the amplitude of the normal modes from the transport in each layer using Eq. (A.10) and apply the OBC to each mode. The amplitudes for each mode on the boundary are then transformed back using Eq. (A.9). This calculation involves two matrix multiplications and is fairly fast. However, note that the calculation of these matrices requires finding eigenvalues and eigenvectors as well as inverting an $N \times N$ matrix. For this reason we use a time- and space-independent reference state, so it is only done once. In cases where the stratification changes with space and time, the normal mode matrices should in principle be recalculated during the integration.

Appendix B. Derivation of characteristic open boundary conditions

Below we will illustrate how the method of characteristics (e.g. Thompson, 1990) can be applied to an open boundary condition. We will use the linear shallow water equations on an f-plane:

$$\frac{\partial U}{\partial t} - fV = -gH_0\frac{\partial \eta}{\partial x} \tag{B.1}$$

$$\frac{\partial V}{\partial t} + fU = -gH_0\frac{\partial \eta}{\partial y} \tag{B.2}$$

$$\frac{\partial \eta}{\partial t} = -\frac{\partial U}{\partial x} - \frac{\partial V}{\partial y} \tag{B.3}$$

where the notation is given in Section 2. We can write equations Eqs. (B.1), (B.2) and (B.3) in matrix form:

$$\begin{pmatrix} U \\ V \\ \eta \end{pmatrix}_t + \underline{\mathbf{A}}\begin{pmatrix} U \\ V \\ \eta \end{pmatrix}_x + \underline{\mathbf{B}}\begin{pmatrix} U \\ V \\ \eta \end{pmatrix}_y + \underline{\mathbf{C}} = 0 \tag{B.4}$$

where the subscript denotes differentiation and the coefficient matrices A, B and C are given by:

$$A = \begin{bmatrix} 0 & 0 & c^2 \\ 0 & 0 & 0 \\ 1 & 0 & 0 \end{bmatrix} \tag{B.5}$$

$$B = \begin{bmatrix} 0 & 0 & 0 \\ 0 & 0 & c^2 \\ 0 & 1 & 0 \end{bmatrix} \tag{B.6}$$

$$C = \begin{pmatrix} -fV - F \\ fU - G \\ 0 \end{pmatrix} \tag{B.7}$$

Each direction will be considered separately. For the x-direction, we have:

$$\begin{pmatrix} U \\ \eta \end{pmatrix}_t + A' \begin{pmatrix} U \\ \eta \end{pmatrix}_x + C' = 0 \tag{B.8}$$

where:

$$A' = \begin{bmatrix} 0 & c^2 \\ 1 & 0 \end{bmatrix} \tag{B.9}$$

and:

$$C' = \begin{pmatrix} -fV - F \\ \partial V / \partial y \end{pmatrix} \tag{B.10}$$

The eigenvalues for A' are $\pm c$. We will select a pair of eigenvectors:

$$\begin{pmatrix} -c \\ 1 \end{pmatrix} \text{ and } \begin{pmatrix} c \\ 1 \end{pmatrix} \tag{B.11}$$

and define a matrix S which consists of these eigenvectors and its inverse:

$$S = \begin{bmatrix} c & -c \\ 1 & 1 \end{bmatrix} \text{ and } S^{-1} = \begin{bmatrix} 1/2c & 1/2 \\ -1/2c & 1/2 \end{bmatrix} \tag{B.12}$$

It is easily seen that we can diagonalize A using these matrices:

$$S^{-1} A S = \begin{bmatrix} c & 0 \\ 0 & -c \end{bmatrix} = \Lambda \tag{B.13}$$

If we apply S^{-1} to Eq. (B.8) we get:

$$\begin{bmatrix} 1/2c & 1/2 \\ -1/2c & -1/2 \end{bmatrix} \begin{pmatrix} U \\ \eta \end{pmatrix}_t + \mathscr{L} + S^{-1} C' = 0 \tag{B.14}$$

where the characteristic vector, $\mathscr{L}$, is defined as in Thompson (1990), that is:

$$\mathscr{L} = \begin{pmatrix} \mathscr{L}_1 \\ \mathscr{L}_2 \end{pmatrix} = \begin{bmatrix} 1/2 & C/2 \\ 1/2 & -C/2 \end{bmatrix} \begin{pmatrix} U \\ \eta \end{pmatrix}_x$$

$$= \begin{pmatrix} 1/2(U + c\eta)_x \\ 1/2(U - c\eta)_x \end{pmatrix} \tag{B.15}$$

After finding the characteristic Eq. (B.15), we now transform Eq. (B.14) back by applying S to Eq. (B.8) we get. We can write:

$$U_t + c(\mathscr{L}_1 - \mathscr{L}_2) - fV - F = 0 \tag{B.16}$$

$$\eta t + (\mathscr{L}_1 + \mathscr{L}_2) + V_y = 0 \tag{B.17}$$

At a right boundary, an outgoing wave propagates with the velocity $+c$ and an incoming (i.e. reflected) wave propagates with the velocity $-c$. We do not want a reflected wave, so we set:

$$\mathscr{L}_2 = \tfrac{1}{2}(U - c\eta)_x = 0 \tag{B.18}$$

on boundary. Using this in Eqs. (B.16) and (B.17), we have on the right boundary:

$$\frac{\partial \tilde{U}}{\partial t} = -\tfrac{1}{2} c^{(k)} \frac{\partial}{\partial x} \left(\tilde{U} + c^{(k)} \tilde{\eta} \right) + f\tilde{V} + \tilde{F} \tag{B.19}$$

$$\frac{\partial \tilde{\eta}}{\partial t} = -\tfrac{1}{2} \frac{\partial}{\partial x} \left(\tilde{U} + c^{(k)} \tilde{\eta} \right) - \frac{\partial \tilde{V}}{\partial y} \tag{B.20}$$

where $\hat{\Phi}$ indicates that the amplitude of the vertical mode k of a variable Φ rather than the amplitude for each layer should be used in the stratified case. For a left boundary we get equations similar to Eqs. (B.19) and (B.20). In the numerical implementation, we only need Eq. (B.19) since the pressure term Eq. (8) can be calculated directly. There are several possibilities for computing the terms in Eq. (B.19). Best results were in general obtained when they were evaluated at time level n and as close to the boundary as possible. On the staggered C-grid, this implies that the two terms with spatial derivatives are computed at positions one half grid cell apart. When additional velocity points were added to center this estimate, a slight improvement in the solution was observed for outflow conditions, while it deteriorated for inflow conditions. Since the averaging results in an upstream estimate for outflow conditions, and a downstream estimate inflow conditions, this could perhaps be expected.

References

Arakawa, A., Lamb, V.R., 1977. Computational design of the basic dynamical processes of the UCLA general circulation model. Methods in Computational Physics, vol. 17. Academic Press, New York, pp. 173–265.

Asselin, R., 1972. Frequency filter for time integrations. Mon. Weather Rev. 100, 487–490.

Beardsley, R.C., Haidvogel, D.B., 1981. Model studies of the wind-driven transient circulation in the Middle Atlantic Bight, Part 1. Adiabatic boundary conditions. J. Phys. Oceanogr. 11, 355–375.

Beckmann, A., Böning, C.W., Köberle, C., Willebrand, J., 1994. Effects of increased horizontal resolution in a simulation of the North Atlantic Ocean. J. Phys. Oceanogr. 24, 326–344.

Camerlengo, A.L., O'Brien, J.J., 1980. Open boundary conditions in rotating fluids. J. Comput. Phys. 35, 12–35.

Chapman, D.C., 1985. Numerical treatment of cross-shelf open boundaries in a barotropic coastal ocean model. J. Phys. Oceanogr. 15, 1060–1075.

Cooper, C., Thompson, J.D., 1989. Hurricane-generated currents on the outer continental shelf 2. Model sensitivity studies. J. Geophys. Res. 94, 12540–12554.

Csanady, G.T., 1982. Circulation in the Coastal Ocean, Reidel, Boston, 279 pp.

Davies, H.C., 1976. A lateral boundary formulation for multi-level prediction models. Quart. J. R. Meteorol. Soc. 102, 405–418.

Davies, H.C., 1983. Limitations on some common lateral boundary schemes used in regional NWP models. Mon. Weather Rev. 11, 1002–1012.

Engedahl, H., 1995. Use of the flow relaxation scheme in a three-dimensional baroclinic ocean model with realistic topography. Tellus 47A, 365–382.

Engquist, B., Majda, A., 1977. Absorbing boundary conditions for the numerical simulation of waves. Math. Comput. 31, 629–651.

Gill, A.E., 1982. Atmosphere–Ocean Dynamics. Academic Press, London, 662 pp.

Givoli, D., 1991. Non-reflecting boundary conditions. J. Comput. Phys. 94, 1–29.

Givoli, D., 1992. Numerical Methods for Problems in Infinite Domains. Elsevier, Amsterdam, 299 pp.

Hedley, M., Yau, M.K., 1988. Radiation boundary conditions in numerical modeling. Mon. Weather Rev. 116, 1721–1736.

Hedstrom, G.W., 1979. Nonreflecting boundary conditions for nonlinear hyperbolic systems. J. Comput. Phys. 30, 222–237.

Israeli, M., Orzag, S.A., 1981. Approximation of radiation boundary conditions. J. Comput. Phys. 41, 115–135.

Jensen, T.G., 1991. Modeling the seasonal undercurrents in the Somali Current system. J. Geophys. Res. 96, 22151–22167.

Jensen, T.G., 1993. Equatorial variability and resonance in a wind-driven Indian Ocean Model. J. Geophys. Res. 98, 22533–22552.

Jensen, T.G., 1996. Artificial retardation of barotropic waves in layered ocean models. Mon. Weather Rev. 124, 1272–1283.

Larsen, J., Darcy, H., 1983. Open boundaries in short wave simulations —a new approach. Coastal Eng. 7, 285–297.

Lighthill, M.J., 1969. Dynamic response of the Indian Ocean to onset of the Southwest Monsoon. Philos. Trans. R. Soc. London A 265, 45–92.

Martinsen, E.A., Engedahl, H., 1987. Implementation and testing of a lateral boundary scheme as an open boundary condition in a barotropic ocean model. Coastal Eng. 11, 603–627.

Miller, M.J., Thorpe, A.J., 1981. Radiation conditions for the lateral boundaries of limited-area numerical models. Quart. J. R. Meteorol. Soc. 107, 615–628.

Nitta, T., 1964. On the reflective computational wave caused by the outflow boundary condition. J. Meteorol. Soc. Jpn. 42, 274–276.

Oey, L.-Y., Chen, P., 1992. A model simulation of circulation in the northeast Atlantic shelves and seas. J. Geophys. Res. 97, 20087–20115.

Oliger, J., Sundström, A., 1978. Theoretical and practical aspects of some initial boundary value problems in fluid dynamics. SIAM J. Appl. Math. 35, 419–446.

Orlanski, I., 1976. A simple boundary condition for unbounded hyperbolic flows. J. Comput. Phys. 21, 251–269.

Poinsot, T.J., Lele, S.K., 1992. Boundary conditions for direct simulations of compressible viscous flows. J. Comput. Phys. 101, 104–129.

Raymond, W.H., Kuo, H.L., 1984. A radiation condition for multi-dimensional flows. Quart. J. R. Meteorol. Soc. 110, 535–551.

Røed, L.P., Cooper, C.K., 1986. Open boundary conditions in numerical ocean models. In: O'Brien, J.J. (Ed.), Advanced Physical Oceanographic Numerical Modelling. Reidel, Dordrecht, pp. 411–436.

Røed, L.P., Cooper, C.K., 1987. A study of various boundary conditions for wind-forced barotropic numerical ocean models. In: Nihoul, J.C.J., Jamart, B.N. (Eds.), Three-dimensional Models of Marine and Estuarine Dynamics. Elsevier, Amsterdam, pp. 305–335.

Røed, L.P., Smedstad, O.M., 1984. Open boundary conditions for forced waves in a rotating fluid. SIAM J. Sci. Stat. Comput. 5, 414–426.

Sarmiento, J.L., 1986. On the North and Tropical Atlantic heat balance. J. Geophys. Res. 91, 11677–11689.

Semtner, A.J., Chervin, R.M., 1992. Ocean general circulation from a global eddy-resolving model. J. Geophys. Res. 97, 5493–5550.

Slørdal, L.H., Martinsen, E.A., Blumberg, A.F., 1994. Modeling the response of an idealized coastal ocean to a traveling storm and to flow over bottom topography. J. Phys. Oceanogr. 24, 1689–1705.

Smith, W.D., 1974. A non-reflecting plane boundary condition for wave propagation problems. J. Comput. Phys. 15, 492–503.

Stevens, D.P., 1991. The open boundary condition in the United Kingdom Fine-Resolution Antarctic Model. J. Phys. Oceanogr. 21, 1494–1499.

Thompson, K.W., 1987. Time-dependent boundary conditions for hyperbolic systems. J. Comput. Phys. 68, 1–24.

Thompson, K.W., 1990. Time-dependent boundary conditions for hyperbolic systems, II. J. Comput. Phys. 89, 436–461.